A meshless and binless approach to compute statistics in 3D Ensemble PTV

Manuel Ratz[1,2,*] and Miguel Alfonso Mendez[1]

1: Environmental and Applied Fluid Dynamics, von Karman Institute for Fluid Dynamics, Waterloosesteenweg 72, Sint-Genesius-Rode, 1640, Belgium

2: Aero-Thermo-Mechanics Lab., Université Libre de Bruxelles, Avenue F. D. Roosevelt, Brussels, 1050, Belgium

*Corresponding author: manuel.ratz@vki.ac.be

Keywords: RBF, meshless algorithm, PTV, turbulent statistics, data assimilation.

ABSTRACT

We propose a method to obtain super-resolution of turbulent statistics for three-dimensional ensemble particle tracking velocimetry (EPTV). Our approach is "meshless" because it does not require a grid to compute derivatives, and it is "binless" because it does not require bins to compute local statistics. The method combines the constrained radial basis function (RBF) formalism introduced in Sperotto et al. (Meas Sci Technol, 33:094005, 2022) with a kernel estimate approach for the ensemble average of the RBF regressions. The computational cost for the RBF regression is alleviated with the partition of unity method (PUM). We compare the newly proposed method with traditional binning-based approaches such as Gaussian weighting (Agüí and Jiménez, JFM, 185:447-468, 1987) and local polynomial fitting (Agüera et al, Meas Sci Technol, 27:124011, 2016). The results on experimental data of an underwater jet show a better resolution of spatial gradients of turbulent stresses while at the same time yielding an analytical expression which results in super-resolution of statistical quantities.

1. Introduction

Much research has focused on developing three-dimensional measurement techniques for all three velocity components (3D3C).The first popular technique was tomographic particle image velocimetry (Elsinga et al., 2006, Tomo PIV), but in recent years particle tracking velocimetry (Dabiri & Pecora, 2019, PTV) has gained more attention. This is because of the spatial averaging inherent to PIV methods, which leads to a lower accuracy compared to PTV (Kähler et al., 2012; Kähler et al., 2016; Schröder & Schanz, 2023). Yet, PTV data is inherently only available in the scattered points and thus requires further post-processing to compute spatial derivatives or flow statistics. These operations usually require mapping the scattered data onto uniform grids.

For instantaneous fields, advanced interpolation methods allow to include physical priors in the form of the Navier-Stokes and continuity equations. This enhances increases the range of resolved length scales and yields either the velocity field interpolated onto an Eulerian grid or an analytical expression of the velocity field that can be sampled at every point (see Sciacchitano et al. (2022), among others).

For statistical fields, such as mean flow fields and Reynolds stresses, a common approach is ensemble PTV (Kähler et al., 2012, EPTV). In EPTV, all vectors from different snapshots are combined to give a dense cloud of vectors. This dense cloud is then interrogated in small regions, referred to as bins, within which statistics can be considered spatially homogeneous. However, this binning also introduces modulation effects due to spatial inhomogeneities and unresolved mean flow gradients.

These effects can be mitigated by applying a Gaussian weight to the data within the bin (Agüí & Jiménez, 1987), which reduces the influence of points outside the bin center but also slows down convergence. Another approach is to perform a local polynomial fit within the bin (Agüera et al., 2016) and subtract the analytical mean to reduce the effects of unresolved mean flow gradients. However, all binning-based approaches inherently only yield the data in the center points of the bin, meaning that the data is only available on the specific binning grid. Moreover, the mean flow field and the Reynolds stresses are not guaranteed to be smooth nor to respect physical priors such as the continuity of the mean flow.

In this work, we extend the existing approaches to compute statistics for turbulent flows through radial basis functions (RBFs). RBFs yield analytical expressions and have been used in many different applications for fluid mechanics (see Karri et al. (2009); Casa & Krueger (2013); Ratz et al. (2022), among others). In this work, we use them directly on the EPTV cloud. We show through simple derivations that an RBF regression of the ensemble of points results in the statistical mean of this ensemble. We use this property to compute mean flow and Reynolds stresses with two successive RBF regressions. Our method is "meshless" because it works on the scattered points directly with no need to interpolate onto grids and "binless" because it acts on the ensemble cloud with no need to modulate statistics within subsets of the domain. This reduces user intervention and provides, as a byproduct, also an analytic expression of the statistical moments. Moreover, the RBFs allow us to visualize the statistics on any grid and to compute derivatives analytically.

The rest of this article is structured as follows. First, we give a brief overview of the RBF regression in section 2 and develop different methods to compute flow statistics. We validate the methods with a 3D PTV experimental characterization of an underwater jet described in section 3 and compare the methods to the existing binning approaches in section 4. Finally, conclusions are drawn in section 5.

2. Methodology

2.1. Fundamendals of RBF approximation

In this work, we consider Gaussian RBFs of the form:

$$\phi_k(\mathbf{x}|\mathbf{x}_{c,k}, c_k) = \exp\left[-c_k^2||\mathbf{x} - \mathbf{x}_{c,k}||^2\right], \tag{1}$$

where $\mathbf{x} = (x, y, z)$ is the coordinate where the basis is evaluated, $\mathbf{x}_{c,k} = (x_{c,k}, y_{c,k}, z_{c,k})$ and c_k are the k-th collocation point and shape parameter of the basis, respectively. In the following, we shorten the notation to $\phi_k(\mathbf{x}|\mathbf{x}_{c,k}, c_k) = \phi_k(\mathbf{x})$.

For the approximation, we express a velocity field $U(X)$ as a linear combination of RBFs:

$$U(X) = \begin{bmatrix} u(X) \\ v(X) \\ w(X) \end{bmatrix} \approx \begin{bmatrix} \Phi_b(X) & \mathbf{0} & \mathbf{0} \\ \mathbf{0} & \Phi_b(X) & \mathbf{0} \\ \mathbf{0} & \mathbf{0} & \Phi_b(X) \end{bmatrix} \begin{bmatrix} w_u \\ w_v \\ w_w \end{bmatrix} = \Phi(X)W, \tag{2}$$

where $\Phi_b(X; X_c, c)$ collects the n_b RBFs in its columns, X is an arbitrary set of sample points, and the entries of $W = (w_u, w_v, w_w) \in \mathbb{R}^{3n_b}$ collect all the weights.

From experimental PIV or PTV measurements, we obtain a set of n_p data points $X^\star \in \mathbb{R}^{n_p}$ in which we have our target function $U^\star = (u^*, v^*, w^*)$. In classic machine learning literature, we refer to these points as training data (Bishop, 2011). Since there usually are more training points than basis functions, the optimal weights are found via least square formulation:

$$W = \left[\Phi(X)^T\Phi(X) + \alpha I\right]^{-1}\Phi(X)^T U^\star, \tag{3}$$

where $\alpha \in \mathbb{R}$ is the regularization parameter of the Ridge Regression and I is the identity matrix of appropriate size (Saleh et al., 2019). With these weights, the function approximation in equation (2) provides a continuous and differentiable representation of the field $U = (u, v, w)$ that can be sampled on an arbitrary grid.

2.2. From ensembles of RBFs to RBF of the ensemble

Let us consider a statistically stationary and ergodic velocity field $\mathbf{u}(\mathbf{x})$. The sample at any location $\mathbf{x}$ depends on the joint probability density function (pdf) $f_u(\mathbf{x}, U)$ so that we can define the mean field from the expectation operator:

$$\langle u\rangle(\mathbf{x}) = \mathbb{E}\{\mathbf{u}(\mathbf{x})\} = \int_{-\infty}^{\infty} \mathbf{u}(\mathbf{x}) f_u(\mathbf{x}, \mathbf{u}) \mathrm{d}\mathbf{u}. \tag{4}$$

We now introduce our RBF approximation from (2) into this integral. Furthermore, we perform a change of variables from $\mathbf{u}$ to W, where the Jacobian is $\mathrm{d}\mathbf{u}/\mathrm{d}W = \mathbf{\Phi}(\mathbf{x})$. Together, this leads to:

$$\langle \mathbf{u} \rangle(\mathbf{x}) = \int_{-\infty}^{\infty} \mathbf{\Phi}(\mathbf{x}) W f_u(\mathbf{x}, \mathbf{\Phi}(\mathbf{x})) \mathrm{d}\mathbf{u} = \mathbf{\Phi}(\mathbf{x}) \int_{-\infty}^{\infty} W f_W(W) \mathrm{d}W = \mathbf{\Phi}(\mathbf{x}) \langle W \rangle, \tag{5}$$

with $f_W(W) = f_u(\mathbf{x}, \mathbf{u})\mathbf{\Phi}(\mathbf{x})$. Thus, we can reformulate an averaging of the joint pdf in space and velocity (eq. (4)) with an averaging over the weights from the regression of multiple PTV snapshots. The advantage is that the RBFs for the individual regressions can have the same collocation point whereas the scattered PTV data is different in each snapshot. We now expand this expression for the weight average according to $\langle W \rangle \approx W_A = \sum_{j=1}^{n_t} W_j$, where W_j are the weights from the training on each of the n_t snapshots. We introduce the solution of the least squares problem (3) and obtain:

$$W_A = \frac{1}{n_t} \sum_{j=1}^{n_t} \left(\mathbf{\Phi}\left(X^{(j)}\right)^T \mathbf{\Phi}\left(X^{(j)}\right) + \alpha I \right)^{-1} \mathbf{\Phi}^T\left(X^{(j)}\right) U^{(j)}, \tag{6}$$

where $X^{(j)}$ and $U^{(j)}$ are the training data of the jth snapshot. This gives an approximation of the weight average $\langle W \rangle$ given that the training of every snapshot is successful. However, to circumvent this requirement, we propose to perform a single regression which uses the *ensemble* X_E, U_E of training points, instead of solving n_t individual regressions.

The idea is to link the ensemble bases $\mathbf{\Phi}_E = \mathbf{\Phi}(X_E)$ to the projections $\mathbf{\Phi}^T\left(X^{(j)}\right) U^{(j)}$ and correlations $\mathbf{\Phi}\left(X^{(j)}\right)^T \mathbf{\Phi}\left(X^{(j)}\right)$ of the individual snapshots:

$$\sum_{j=1}^{n_t} \mathbf{\Phi}_{(j)}^T \mathbf{\Phi}_{(j)} = \mathbf{\Phi}_E^T \mathbf{\Phi}_E \in \mathbb{R}^{n_b \times n_b} \quad \text{and} \quad \sum_{j=1}^{n_t} \mathbf{\Phi}_{(j)}^T U^{(j)} = \mathbf{\Phi}_E^T U_E \in \mathbb{R}^{n_b \times n_b}. \tag{7}$$

We note that the correlation of the ensemble basis is computed from possibly millions of points in the ensemble. In that case, the matrix becomes independent of the sample points and can be linked to a kernel function:

$$\kappa\left(X^{(i)}, X^{(j)}\right) = \mathbf{\Phi}\left(X^{(i)}\right)^T \mathbf{\Phi}\left(X^{(j)}\right). \tag{8}$$

While not currently implemented, this idea can be exploited in the future to compute the correlation matrix with a function evaluation instead of a matrix multiplication. If we further assume that each snapshot has sufficiently dense sampling, each snapshot matrix is an approximation of the ensemble correlation matrix:

$$\mathbf{\Phi}_{(j)}^T \mathbf{\Phi}_{(j)} \approx \frac{1}{n_t} \mathbf{\Phi}_E^T \mathbf{\Phi}_E. \tag{9}$$

We can insert this assumption into (6) to approximate the average weights:

$$\langle W \rangle \approx W_A \approx W_E = \left(\Phi^T(X_E)\Phi X_E) + \alpha I \right)^{-1} \Phi_E^T U_E \,. \tag{10}$$

Therefore, a single, large regression can be used to obtain the weights for the mean of the velocity field.

2.3. Meshless and binless statistics in EPTV

An RBF regression of an ensemble can be used to compute the statistical mean of a random field. Therefore, we now use it to compute first and second-order moments for turbulent flows. Here, we propose three different RBF-based methods to compute statistics. The flowchart of the different methodologies is shown in figure 1, where the color of each arrow in between steps corresponds to the label in the bottom left corner of the figure.

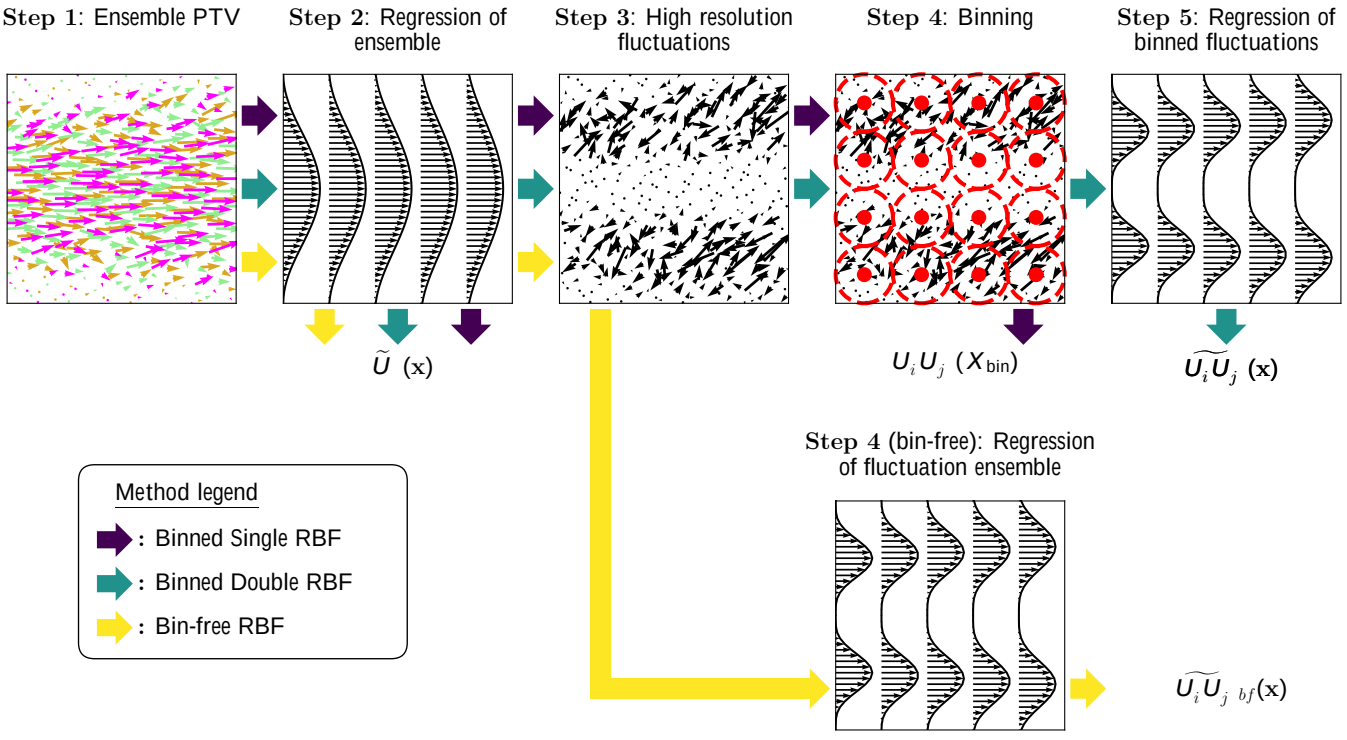

Figure 1. Flowchart explaining the processing pipeline of the three proposed RBF-based methods. The colors of the arrows correspond to each of the three methods according to the legend. All three methods subtract the global mean field analytically and then extract higher order statistics using (1) binning (Binned Single RBFs, purple) (2) binning and RBF regression (Binned Double RBF, teal), or (3) only an RBF regression (Bin-free Double RBF, yellow).

- **Step 1**. The starting point for all methods is an ensemble flow field, obtained by merging many snapshots of the flow. This is indicated in figure 1, where the colors correspond to snapshots at different times.

- **Step 2**. For all methods, the mean flow is computed with a single regression of the ensemble. Given that the ensemble typically contains millions of points, the partition of unity method (PUM) is used to handle the computational cost. With RBF-PUM, the domain is split into subdomains on which a local regression is computed and the global solution is constructed from a linear combination of local solutions (see for example Cavoretto (2015); Larsson et al. (2017); Ratz et al. (2022); Li & Pan (2024) for implementation details). Linear physical constraints, like a divergence-free flow and Dirichlet and Neumann boundary conditions are also enforced within this framework. The result is an analytical mean flow field:

$$\langle \bar{U} \rangle(\mathbf{x}) = \mathrm{RBF}(X_E, U_E)\,. \tag{11}$$

- **Step 3**. The function (11) is used to compute the ensemble of velocity fluctuations by subtracting the mean field $\langle \bar{U} \rangle(X_E)$ to the ensemble field:

$$U'(X_E) = U_E - \langle \bar{U} \rangle(X_E)\,. \tag{12}$$

  This field is then used to compute all the products $U_i' U_j'(X_E)$, that are required by all methods in the following steps. This is the last common step for the three methods.

  Binned Single RBF

- **Step 4**. This method now interrogates the ensemble fields of products $U_i' U_j'(X_E)$ with a standard binning process. The process is similar to the polynomial fitting from Agüera et al. (2016) as it also only yields statistics on the discrete binning grid X_{bin}. The main advantage over the polynomial fitting is that the solution is globally smooth and the mean flow is obtained with constraints.

  Binned Double RBF

- **Step 5**. This method builds on the binning grid from **Step 4** of Binned Single RBF with a second regression:

$$\langle \bar{U_i} \bar{U_j'} \rangle(\mathbf{x}) = \mathrm{RBF}(X_{\mathrm{bin}}, \langle U_i' U_j' \rangle(X_{\mathrm{bin}}))\,. \tag{13}$$

  This regression gives an analytical expression of the Reynolds stresses and smoothes noisy fields if the number of vectors within the bin is too small. Thus, fewer samples are needed for statistical convergence. This additional regression can also be applied to classic binning methods (Agüera et al., 2016; Godbersen & Schröder, 2020), to accelerate convergence.

  Bin-Free RBF

- **Step 4** (bin-free). The bin-free approach deviates from the former two methods after **Step 3**. The method works on the ensemble fields of products $U_i' U_j'(X_E)$ without binning, replacing the ensemble operators with the spatial RBF regression of the ensemble:

$$\langle U_i' U_j' \rangle_{bf}(\mathbf{x}) = \mathrm{RBF}(X_E, U_i' U_j'(X_E)), \tag{14}$$

where the subscript $'bf'$ is used to distinguish the output of (14) from the output in (13). The main advantage concerning the previous approach is to bypass the averaging effects of the binning. This step is more expensive than **Step 5** of Binned Double RBF as there are more data points than binning points. However, matrices from the mean flow regression can be reused, and the cost becomes manageable with RBF-PUM.

3. Experimental setup

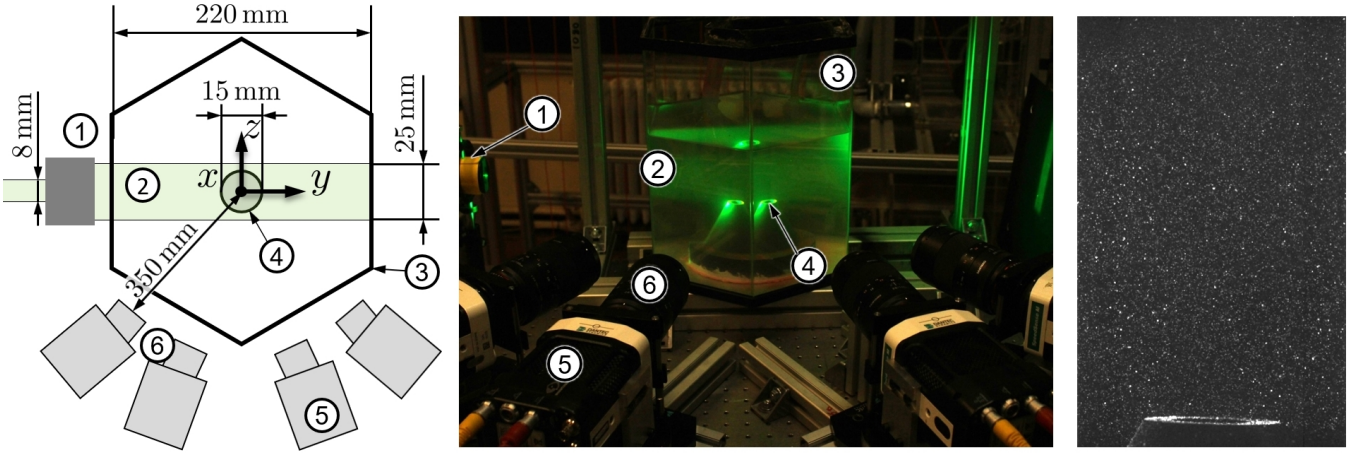

Figure 2. (a) Top-down sketch of the experimental facility with the right-handed coordinate system and (b) image of the facility during the acquisition. Laser light (1) enters the top-hat illumination optics to produce a volumetric illumination (2) which enters the hexagonal tank (3). The illumination is centered above the jet nozzle (4) which is located at the bottom of the tank. Four high-speed cameras (5) with 100 mm objectives (6) record the jet in an arc that covers approximately 125°; (c) example of an acquired raw image for the left-most camera.

The proposed methods to compute turbulent statistics are validated with 3D PTV measurements of an underwater jet. The exit diameter D of the nozzle was 15 mm and the exit velocity U_0 was $0.45\,\mathrm{m\,s^{-1}}$ which results in a diameter-based Reynolds number of 6750. The measurement setup is sketched in figure 2(a). The jet was illuminated from the side through top-hat illumination optics from Dantec Dynamics which had an aspect ratio of 5:1. Four SpeedSense M310 cameras with a resolution of 1280×800 px recorded the flow in a time-resolved manner. The cameras were equipped with 105 mm Samyang Macro Objectives and long-pass filters to suppress reflected laser light. The cameras recorded the illuminated volume in a region of ($4.5D \times 2.5D \times 1.3D$) in

($x \times y \times z$). Red fluorescent microspheres with a diameter ranging from $45 - 53\,\mu m$ were used as tracer particles. The particles were illuminated with a Quantronix Darwin Duo 527-80-M laser which produced 25 mJ per pulse.

Image acquisition and processing were carried out in Dynamic Studio 8.0. A total of 2000 images were acquired at a frequency of 1000 Hz. Fig. 2(b) shows the facility during the acquisition and an example of a raw camera image is shown in figure 2(c). The images were preprocessed with a mean background subtraction and subsequent thresholding. At every timestep, the voxel volume was reconstructed with the SMART algorithm (Atkinson & Soria, 2009), and four-frame particle tracking was carried out on the voxel volumes to obtain particle tracks (Kitzhofer et al., 2009). To suppress outliers and ghost particles only tracks with a length greater than 5 timesteps were accepted as valid. The particle ensemble was further processed with universal outlier detection (Westerweel & Scarano, 2005) resulting in a total of 3.35 Mio particles.

4. Results

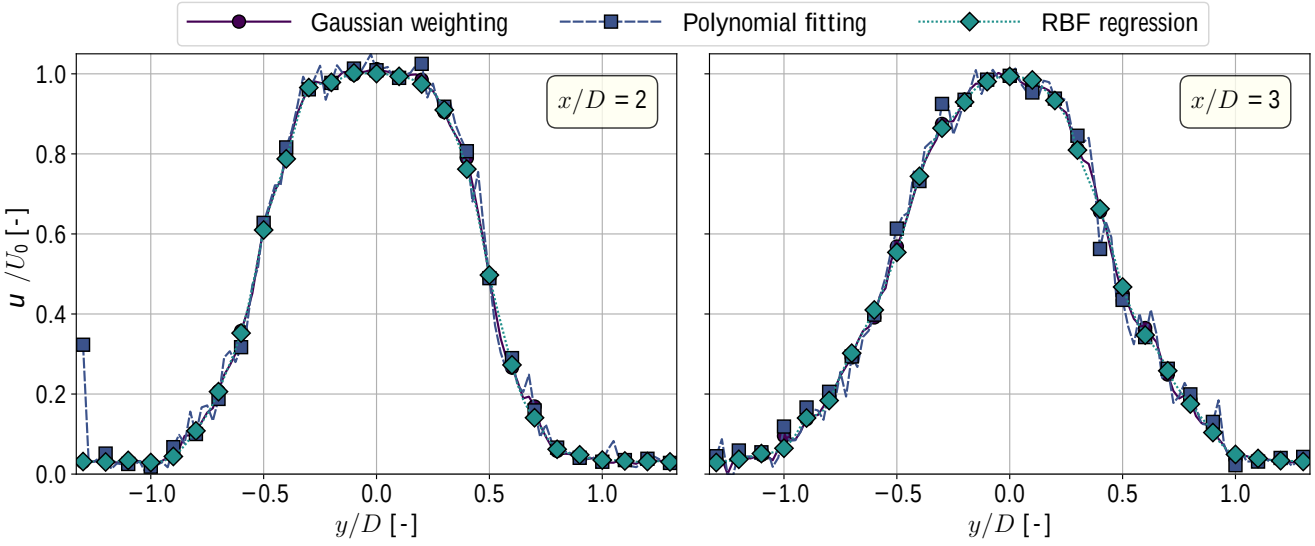

Figure 3. Resulting mean velocity profile $\langle u \rangle / U_0$ extracted at $z/D = 0$, $x/D = 2$ (left) and $z/D = 0$, $x/D = 3$ (right). The three curves correspond to the Gaussian weighting (●, Agüí & Jiménez (1987)), local polynomial fitting (■, Agüera et al. (2016)) and the RBF regression of the ensemble (◆).

The ensemble is processed with approximately 77 000 equally spaced RBFs aranged on a uniform grid ($75 \times 49 \times 21$) in ($x \times y \times z$). A divergence-free flow is constrained on the outer hull of the volume along ($81 \times 53 \times 23$) points in ($x \times y \times z$) and a divergence-free flow is penalized in every data point. All RBF regressions use these same parameters. The binning diameter for the binning-based RBF and classic methods uses isotropic bins with a diameter $D_b = 0.2D$, where the Gaussian weighting uses a standard deviation $\sigma = D_b/3$.

Figure 3 shows two mean velocity profiles extracted at $z/D = 0$, $x/D = 2$ (left) and $z/D = 0$, $x/D = 3$ (right). The different colors and markers denote the Gaussian weighting, the polynomial fitting, and the RBF regression. It can be seen that the profiles almost completely collapse. Slight differences of approximately 2 % of the normalized maximum velocity are visible in the core of the jet. The curves between all three methods appear almost identical except for some spikes for the polynomial fitting, which happen because there are too few vectors in these bins. The strong potential core is visible, and the profiles tend toward self-similarity.

While all three methods yield a similar velocity profile, the RBF regression has the advantage of being mesh- and binless. The other two methods only yield discrete data in the bin centers, whereas the RBFs yield a continuous expression. This results in analytical spatial derivatives and super-resolution on an arbitrary grid for the purpose of visualizing and comparing the data.

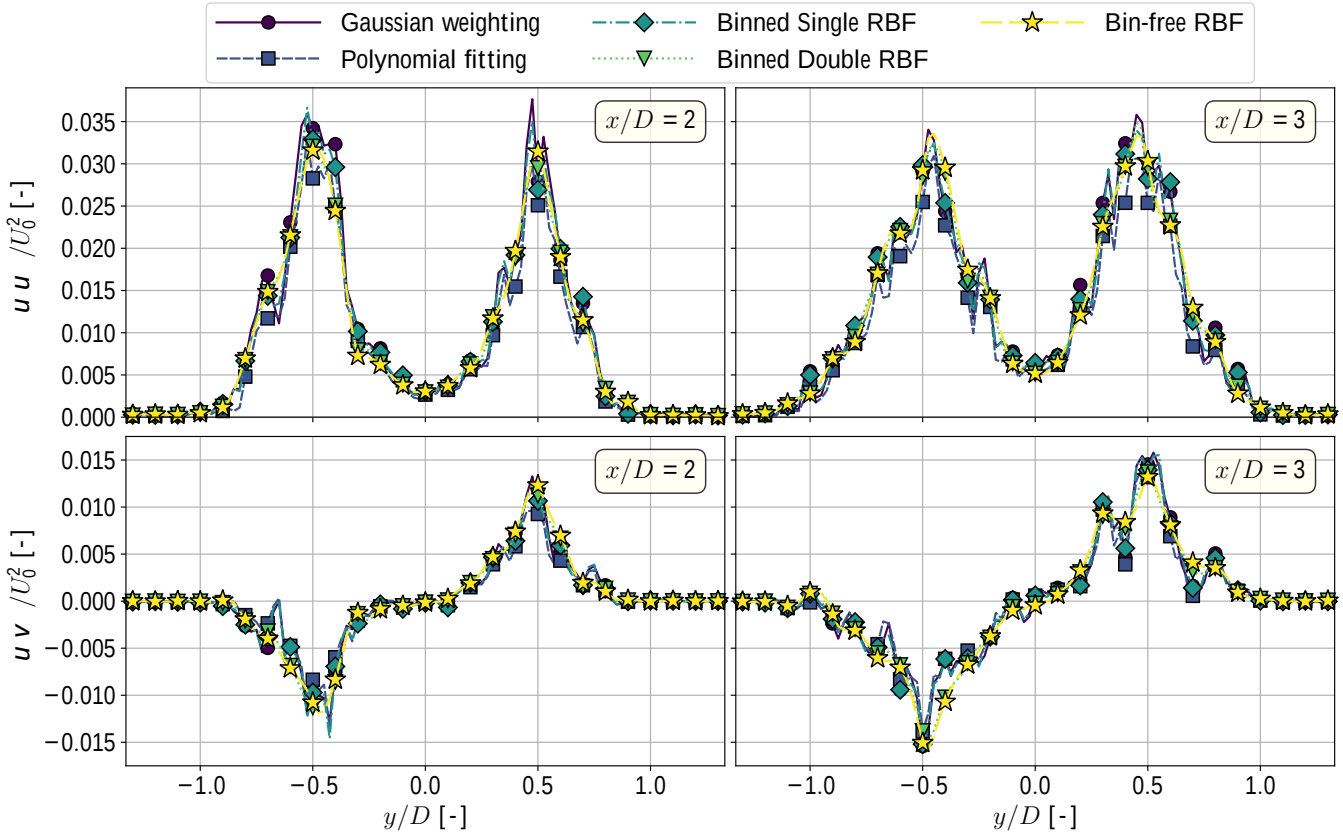

Figure 4. Test case 3. Resulting Reynolds stress profile $\langle u\,u\rangle/U_0^2$ (top) and $\langle u\,v\rangle$ (bottom) extracted at $z/D = 0$, $x/D = 2$ (left) and $z/D = 0$, $x/D = 3$ (right). The five curves correspond to the Gaussian weighting (●, Agüí & Jiménez (1987)), local polynomial fitting (■, Agüera et al. (2016)), Binned Single RBF (◆), Binned Double RBF (▼), and Bin-free RBF (★).

The Reynolds stress profiles at $z/D = 0$, $x/D = 2$ and $z/D = 0$, $x/D = 3$ are respectively shown on the left- and right-hand side of figure 4. The top row shows the normal stress $\langle u'u'\rangle/U_0^2$, while the bottom row shows the shear stress $\langle u'v'\rangle/U_0^2$. The profiles agree with theoretical expectations: the

peak of the profiles occurs at $y/D = 0.5$, the position of the shear layer and the shown normal and shear stress is an even and odd functions, respectively. Compared to the mean flow, the profiles show more noise spikes as higher order statistics require more points for convergence. Among the methods, Binned Double and Bin-free RBF are affected least by this as the regression of the Reynolds stresses yields a globally smooth field. In contrast, the pure binning-based methods only consider the bin data, which can lead to large differences between neighboring bins.

5. Conclusion and Outlook

In this work, we proposed a new method to compute statistics in turbulent flows. Our method uses radial basis functions (RBFs) to give analytical expressions of first and second order moments. The RBFs lead to super-resolution on arbitrary grids and analytical derivatives for all statistical fields (e.g. mean or Reynolds stresses). Different approaches to incorporate the RBFs into the binning process were proposed, with Single Binned RBF being very similar to the existing polynomial fitting (Agüera et al., 2016). The most advanced method completely removes the bins and directly works on the scattered data. Therefore, the method is meshless and binless, requires fewer intermediate steps, and provides faster statistical convergence.

Compared on experimental data of an underwater jet, we show that all of our methods outperform classic Gaussian weighting (Agüí & Jiménez, 1987) and local polynomial fitting (Agüera et al., 2016). Both the mean flow and the Reynolds stress curves almost collapse, and no effects of unresolved mean flow gradients contaminate higher-order statistics. However, our methods yield a globally smooth solution while the polynomial fitting is only locally smooth. Moreover, we can incorporate physical constraints such as a divergence-free flow or no-slip boundary conditions, which improve the regression. Ongoing work uses the analytical expressions of the statistics to integrate the pressure Poisson equation in the Reynolds-Averaged Navier-Stokes framework.

Acknowledgements

This project was mostly carried out in the framework of M. Ratz's Research Master project at the von Karman Institute (VKI), supported by a VKI RM grant. M. Ratz is currently supported by a F.R.S.-FNRS FRIA grant number FC57471. The authors kindly acknowledge Alessia Simonini for her help in setting up and conducting the experiments and David Hess from Dantec Dynamics for the support in setting up the measurement system and helping during the post-processing with Dynamic Studio.

References

Agüera, N., Cafiero, G., Astarita, T., & Discetti, S. (2016). Ensemble 3D PTV for high resolution turbulent statistics. *Measurement Science and Technology*, *27*(12), 124011. doi: 10.1088/0957-0233/27/12/124011

Agüí, J. C., & Jiménez, J. (1987). On the performance of particle tracking. *Journal of Fluid Mechanics*, *185*, 447–468.

Atkinson, C., & Soria, J. (2009, 10). An efficient simultaneous reconstruction technique for tomographic particle image velocimetry. *Experiments in Fluids*, *47*, 553-568. doi: 10.1007/s00348-009-0728-0

Bishop, C. M. (2011). *Pattern Recognition and Machine Learning*. Springer.

Casa, L., & Krueger, P. (2013). Radial basis function interpolation of unstructured, three-dimensional, volumetric particle tracking velocimetry data. *Measurement Science and Technology*, *24*, 065304. doi: 10.1088/0957-0233/24/6/065304

Cavoretto, R. (2015, 04). A numerical algorithm for multidimensional modeling of scattered data points. *Computational & Applied Mathematics*, *34*, 65-80. doi: 10.1007/s40314-013-0104-9

Dabiri, D., & Pecora, C. (2019). *Particle Tracking Velocimetry*. IOP Publishing. doi: 10.1088/978-0-7503-2203-4

Elsinga, G., Scarano, F., Wieneke, B., & Oudheusden, B. (2006). Tomographic Particle Image Velocimetry. *Experiments in Fluids*, *41*, 933-947. doi: 10.1007/s00348-006-0212-z

Godbersen, P., & Schröder, A. (2020). Functional binning: Improving convergence of eulerian statistics from Lagrangian particle tracking. *Measurement Science and Technology*, *31*, 095304. doi: https://doi.org/10.1088/1361-6501/ab8b84

Kähler, C. J., Astarita, T., Vlachos, P. P., Sakakibara, J., Hain, R., Discetti, S., … Cierpka, C. (2016). Main results of the 4th International PIV Challenge. *Experiments in Fluids*, *57*(79), 1-71. doi: 10.1007/s00348-016-2173-1

Karri, S., Charonko, J., & Vlachos, P. P. (2009). Robust wall gradient estimation using radial basis functions and proper orthogonal decomposition (POD) for particle image velocimetry (PIV) measured fields. *Measurement Science and Technology*, *20*(4), 045401. doi: 10.1088/0957-0233/20/4/045401

Kitzhofer, J., Kirmse, C., & Brücker, C. (2009). High Density, Long-Term 3D PTV Using 3D Scanning Illumination and Telecentric Imaging. In C. D. Wolfgang Nitsche (Ed.), *Imaging measurement methods for flow analysis* (Vol. 106, p. 125-134). Springer Berlin, Heidelberg.

Kähler, C. J., Scharnowski, S., & Cierpka, C. (2012). On the resolution limit of digital particle image velocimetry. *Experiments in Fluids*, *52*(6), 1629 - 1639. doi: 10.1007/s00348-012-1280-x

Larsson, E., Shcherbakov, V., & Heryudono, A. (2017). A Least Squares Radial Basis Function Partition of Unity Method for Solving PDEs. *SIAM Journal on Scientific Computing*, *39*(6). doi: 10.1137/17M1118087

Li, L., & Pan, Z. (2024). Three-dimensional time-resolved Lagrangian flow field reconstruction based on constrained least squares and stable radial basis function. *Experiments in Fluids*, *65*, 57. doi: 10.1007/s00348-024-03788-y

Ratz, M., König, J., Mendez, M., & Cierpka, C. (2022). Radial basis function regression of Lagrangian three-dimensional particle tracking data. In *20th International Symposium on Applications of Laser and Imaging Techniques to Fluid Mechanics.*

Saleh, A. K. M. E., Arashi, M., & Kibria, B. M. G. (Eds.). (2019). *Theory of Ridge Regression Estimation with Applications*. Wiley. doi: https://doi.org/10.1002/9781118644478

Schröder, A., & Schanz, D. (2023). 3D Lagrangian Particle Tracking in Fluid Mechanics. *Annual Review of Fluid Mechanics*, *55*(1), 511–540. doi: 10.1146/annurev-fluid-031822-041721

Sciacchitano, A., Leclaire, B., & Schröder, A. (2022). Main results of the analysis of the HOMER Lagrangian Particle Tracking and Data Assimilation database. In *20th International Symposium on Applications of Laser and Imaging Techniques to Fluid Mechanics.*

Westerweel, J., & Scarano, F. (2005). Universal outlier detection for PIV data. *Experiments in Fluids*, *39*, 1096-1100. doi: 10.1007/s00348-005-0016-6